ACADEMIC PRESS

Available online at www.sciencedirect.com
SCIENCE DIRECT®

Journal of Catalysis 215 (2003) 139–150

JOURNAL OF CATALYSIS

www.elsevier.com/locate/jcat

Molecular structure of supported molten salt catalysts for SO_2 oxidation

Antonios Christodoulakis and Soghomon Boghosian *

Department of Chemical Engineering, University of Patras, and Institute of Chemical Engineering and High Temperature Chemical Processes (FORTH/ICE-HT), GR-26500, Patras, Greece

Received 13 September 2002; revised 8 November 2002; accepted 19 November 2002

Abstract

In situ Raman spectroscopy has been used at 350–480 °C in various $SO_2/O_2/H_2O/N_2$ atmospheres to study the molecular structure of the vanadium complexes present in the active liquid phase of industrial supported molten salt sulfuric acid catalysts. The catalytic behavior and deactivation of the studied catalysts has been followed by separate activity measurements. Under oxidizing conditions (O_2, 480 °C) the surface of the catalysts is covered by a molten salt in which the mononuclear $V^VO_2(SO_4)_2^{3-}$ complex (in monomeric or oligomeric form) is predominant. Crystalline sulfate salts are also detected. After being subjected to *activation* (i.e., in an $SO_2/O_2/N_2$ atmosphere at 480 °C), the catalysts take up SO_3 and thereby crystalline sulfate is converted to molten pyrosulfate; the molten phase of the catalysts is shown to consist of $(V^VO)_2O(SO_4)_4^{4-}$ (dimeric or binuclear fragments of oligomers) and $V^VO_2(SO_4)_2^{3-}$. Below a certain temperature, which strongly depends on catalyst composition, the Raman data are indicative of $V^V \rightarrow V^{IV}$ reduction and formation of the molten $V^{IV}O(SO_4)_2^{2-}$ complex, the accumulation of which results in precipitation of V^{IV} crystalline compounds—mainly $K_4(VO)_3(SO_4)_5$—and depletion of the active phase in terms of vanadium. In reducing conditions (i.e., in SO_2/N_2 atmosphere) the $V^V \rightarrow V^{IV}$ reduction and V^{IV} precipitation occur at higher temperature. The low-temperature (i.e., below 420 °C) catalytic activity is related to the stability of vanadium in the +5 state. Mixing of alkali promoters with the inclusion of Cs and/or the presence of H_2O vapors in the feed gas contributes to the ability of the catalysts to stabilize the pentavalent vanadium complexes by preventing their reduction. The molecular structure of the components constituting the active liquid phase of industrial SO_2 oxidation catalysts is studied by in situ Raman spectroscopy for the first time.

Keywords: Sulfuric acid catalyst; SO_2 oxidation; Pyrosulfate melts; Vanadium oxosulfato complexes; Molten salt catalysts; In situ Raman spectra; Vanadia catalysts

1. Introduction

Sources of SO_2 emissions to the atmosphere include mainly coal-fired power generation, sulfuric acid manufacturers, and smelters of nonferrous metals. Production of sulfuric acid is currently performed not only from traditional sulfuric acid plants but also from NO_x and SO_x removal stations, combined with SCR technology such in the so-called Haldor–Topsøe SNOX process [1]. Thus, catalysts for SO_2 oxidation are important for sulfuric acid production as well as for the catalytic removal of SO_2 from industrial off-gases.

The industrial catalyst used for sulfuric acid production, catalyzing the reaction $SO_2 + \frac{1}{2}O_2 \rightarrow SO_3$, is made by calcination of diatomaceous earth, vanadium pentoxide (or other vanadium precursors), and alkali promoters (usually in the form of sulfates or oxides) and has been the subject of numerous research papers dating back to the 1940s [2–5]. However, issues of fundamental significance including the reaction mechanism, the route of catalyst deactivation (experienced as a sudden drop of activity below ∼ 440 °C), and the molecular structure of the species present during the reaction remained unresolved. During the activation process, the catalyst takes up large amounts of SO_3, whereby molten alkali sulfates and pyrosulfates are formed, which dissolve the vanadium salts, and thus, it has been recognized that the active phase of the working catalyst is a *molten salt* mixture [2,3].

In situ real-time spectroscopic characterization of catalytic active centers in vanadium-oxide-based *supported molten salt* catalysts for SO_2 oxidation under gas and temperature conditions of practical importance has been a long-sought goal in catalysis [6]. For years, it was believed that the direct spectroscopic study of the species formed in the liquid phase, which is dispersed in the small pores of the industrial sulfuric acid catalysts, is very difficult [6] and that

* Corresponding author.
E-mail address: bogosian@iceht.forth.gr (S. Boghosian).

0021-9517/03/$ – see front matter
doi:10.1016/S0021-9517(02)00158-6

probably only methods such as NMR [7,8] and ESR [9,10] could be applied. Mastikhin et al., who have initiated application of magnetic resonance techniques to study vanadium catalysts [7,8], were the first who directly showed that under reaction conditions the active catalyst component exists as a melt forming a very thin layer on the surface of the support [11]. ESR spectra [9,10] measured at temperatures up to 500 °C revealed that precipitation of V^{IV} caused deactivation of the catalysts.

Presently, the molten salt/gas system V_2O_5–$M_2S_2O_7$–M_2SO_4/SO_2–O_2–SO_3–N_2 (M = K, Na, Cs, or mixtures of these) at 400–600 °C is considered to be a realistic model of the working industrial sulfuric acid catalyst [6]. Thus, the study of the above mentioned *unsupported* molten salt system enables the determination of the physicochemical properties and the understanding of the chemistry of the active catalytic liquid phase.

Following a landmark article [12] initiating a systematic study of complex formation of V^V in pyrosulfate melts (without the presence of the catalyst carrier), a number of methods including potentiometry, cryoscopy, spectrophotometry, calorimetry, conductometry, cyclic voltammetry, NMR, and Raman spectroscopy have been used to study the V^V complexes in V_2O_5–$M_2S_2O_7$–M_2SO_4 melts [12–20]. Significantly, the catalytic cycle involves only V^V species (binuclear/dimeric complexes) [6,21], while side reactions lead to reduction of V^V to the catalytically inactive V^{IV} (or V^{III}). Arrhenius plots of apparent SO_2 oxidation reaction rates vs $1/T$ invariably exhibit a break at a specific temperature, below which a sudden increase of the apparent activation energy is observed [5,22,23]. Catalytic activity studies of SO_2 oxidation in *unsupported* V_2O_5–$M_2S_2O_7$ (M = K, Na, Cs, or mixtures of these) melts allowed the isolation of precipitating V^{IV} and V^{III} crystalline vanadium compounds below the temperature of the break in the Arrhenius plots of the measured apparent reaction rates [24,25]. Thus, precipitation of V^{IV} and V^{III} crystalline compounds is responsible for the catalyst deactivation, experienced typically below ∼ 440 °C. Depending on the catalyst melt composition and the gas conditions applied, a number of such compounds ($K_4(VO)_3(SO_4)_5$, $Na_2VO(SO_4)_2$, $K_3(VO)_2(SO_4)_4$, β-$VOSO_4$, $KV(SO_4)_2$, etc.) have been isolated and characterized and are referred to as catalyst deactivation products [6,24,25]. It is therefore clear that high catalytic activity is related to the ability of the catalyst to stabilize vanadium in the +5 oxidation state and maintain the $V^V \leftrightarrow V^{IV}$ equilibrium shifted to the left. The complex chemistry of V^{IV} and the equilibrium $V^V \leftrightarrow V^{IV}$ in the molten salt–gas system V_2O_5–$M_2S_2O_7$–M_2SO_4/SO_2–O_2–SO_3–N_2 (M = K, Cs) has been studied by high-temperature VIS/NIR, ESR, potentiometry, and Raman spectroscopy [20,26,27].

Recently, high-temperature Raman spectroscopy has been used for the first time to establish the molecular structure of vanadium oxosulfato complexes present in the *unsupported* V_2O_5–$Cs_2S_2O_7$–Cs_2SO_4/O_2 [18], V_2O_5–M_2SO_4/O_2 (M = K or Cs) [19], and V_2O_5–$M_2S_2O_7$–M_2SO_4/SO_2–O_2 (M = K or Cs) [20] molten salt/gas systems. The obtained information on the structural properties of the V^V and V^{IV} complexes contributed significantly in achieving progress on the mechanistic understanding of SO_2 oxidation [6]. It thus remained to be realized if the molecular structure of vanadium species present in the surface of *supported molten salt* SO_2 oxidation catalysts could be studied by in situ Raman spectroscopy.

The present article reports, for the first time, the results of our endeavors to study a series of working industrial (Haldor Topsøe A/S, Denmark) SO_2 oxidation catalysts by in situ Raman spectroscopy and check if their structural properties can be linked with those of unsupported molten salts studied by us previously [18–20].

2. Experimentals and methods

2.1. Catalysts

The commercial catalysts investigated were VK38, VK58, and VK-WSA, manufactured by Haldor Topsøe A/S, Denmark, and designed for use in the sulfuric acid production process. VK38 is a "classic" industrial SO_2 oxidation catalyst containing Na and K salts as promoters (molar ratio K/Na/V = 3/0.8/1, 6.5% w/w V_2O_5). VK58 is an advanced last-bed (typically) catalyst with improved low-temperature activity based in a mixture of Na, K, and Cs salts as promoters (molar ratio K/Cs/Na/V = 3/1/0.25/1). VK-WSA, although chemically identical to VK38, is based on a modified porous kieselguhr support, designed specifically for use in humid feed gases as in the flue gas desulphurization process (SNOX). The catalyst data and the chemical composition can be seen in Table 1.

2.2. Catalytic activity

Feed gas with a composition similar to dry flue gas (without NO_x) was prepared by mixing SO_2 (99.98% anhydrous), O_2 (99.99%), CO_2 (> 99.7%), and N_2 (99.999%) in an evacuated special steel bottle followed by external heating at the bottom to obtain a uniform gas mixture by convection. The absence of NO_x corresponds to the condition of SO_2 oxidation in the SNOX process, where NO_x has been removed upstream [1]. Wetting of the gas mixture was achieved by bubbling the dry gas to saturation through water contained in two flasks connected in series and immersed in a thermostat at the appropriate temperature. The experimental setup and the procedures used to measure catalytic activity from unsupported and supported molten salt catalysts have been described elsewhere [24,25,28]. The catalysts were crushed to a size of ∼ 1 mm and placed in the reactor flow-cell as described earlier [24]. The reactor cell, made of Pyrex glass [24], was mounted in a double-walled canthal-wire-

Table 1
Composition and temperatures of deactivation, and precipitation for industrial SO_2 oxidation catalysts

Catalyst	Chemical composition (molar)	Mole % V_2O_5 of active phase	Average pore size	T_b (°C)[a]	Apparent activation energy (kcal/mol)	
					$T > T_b$	$T < T_b$
VK38[b]	K/Na/V = 3/0.8/1	20.8	Normal	421	20.9	60.1
VK58[b]	K/Cs/Na/V = 3/1/0.25/1	19.0	Normal	379	15.0	55.6
VK-WSA[b]	K/Na/V = 3/0.8/1	20.8	Small	421	11.7	28.5
VK38[c]	K/Na/V = 3/0.8/1	20.8	Normal	419	16.6	55.5
VK58[c]	K/Cs/Na/V = 3/1/0.25/1	19.0	Normal	382	16.6	56.0
VK-WSA[c]	K/Na/V = 3/0.8/1	20.8	Small	383	16.9	41.2

[a] T_b is the temperature at which the breakpoint in the Arrhenius plots (Fig. 1) and the compound precipitation (V^{IV} and/or V^{III}) occur simultaneously.
[b] Feed gas: 0.2% SO_2, 4.5% O_2, 15% CO_2, and 80.2% N_2.
[c] Feed gas: 0.2% SO_2, 4% O_2, 7% H_2O, 14% CO_2, and 74.8% N_2.

wound quartz tube furnace, where temperature was controlled to within ±2 °C.

2.3. In situ Raman spectra

Approximately 150 mg of the catalyst were crushed and pressed into a self-supporting wafer, which was mounted on a stainless steel adjustable holder in the center of the in situ Raman furnace. The Raman furnace is a kanthal-wound double-walled quartz-glass tube furnace mounted on xyz plate and possesses gas inlets and outlets as well as a thermocouple sheath in contact with the catalyst sample holder. The gases used were SO_2 (99.98% anhydrous), N_2 (99.999%), and O_2 (99.999%) and they were mixed using thermal mass flowmeters. The gas feed consisted of 0.4% SO_2 and 4% O_2 in a balance of N_2 at a total feed flow rate of 25 cm^3/min. Wetting of the $SO_2/O_2/N_2$ mixture could be achieved by bubbling the carrier gas (N_2) to saturation through water contained in flasks immersed in a thermostat as described above.

Raman spectra were excited by using the 488.0-nm line of a Spectra Physics 164 argon ion laser, which was focused on the catalyst wafer by a cylindrical lens and operated at a power level of 25 mW at the sample. The scattered light was collected at 90° (horizontal scattering plane), analyzed with a 0.85-m Spex 1403 double monochromator, and detected by a −20 °C cooled RCA photomultiplier equipped with EG&G photon counting electronics.

Each catalyst sample was treated with flowing O_2 at 480 °C for 1 h in the Raman furnace and in situ Raman spectra were then recorded in O_2 at 480 °C. Subsequently, in situ Raman spectra were obtained in $SO_2/O_2/N_2$, SO_2/N_2, and $SO_2/H_2O/N_2$ from 480 to 350 °C by checking the temperature dependence of the spectra in 20–30 °C intervals. Before the gas atmosphere was changed in the above sequence, the catalyst was cycled by being subjected to oxidation in O_2 at 480 °C and activation in $SO_2/O_2/N_2$ at 480 °C and the Raman spectra corresponding to these conditions were reproduced.

3. Results and discussion

3.1. Catalytic activity

The results of the activity measurements undertaken in the temperature range 350–470 °C for the three industrial catalysts studied in both wet and dry simulated flue gas are displayed in Fig. 1. The dry flue gas used consists of 0.2% SO_2, 4.5% O_2, 15.1% CO_2, and 80.2% N_2, and the wet flue gas of 0.2% SO_2, 4% O_2, 7% H_2O, 14.1% CO_2, and 74.8% N_2. Two regions with low and high activation energy, are observed, crossing each other in a sharp break at a temperature designated as T_b [24], given in Table 1. The apparent activation energies (listed in Table 1) above and below T_b are in agreement with previous studies on unsupported $M_2S_2O_7$–V_2O_5 (M = K, Na, Cs, or mixtures of these) molten salts and supported catalysts [24,25]. We have previously demonstrated that the sudden drop in activity (visualized in Fig. 1 by the break in the Arrhenius plots) is due to precipitation of V^{IV} and/or V^{III} crystalline compounds [24,25] and the following discussion of the in situ Raman spectra will show that this is indeed the case. The data in Fig. 1 and Table 1 show that in dry feed gas conditions the activity loss for the VK58 catalyst occurs at much a lower temperature compared to both VK38 and VK-WSA. As also shown before [25], this is due to the mixing of all three cations and the slightly lower vanadium content in VK58, which lead to higher solubility of the V^{IV} salts, moving T_b toward lower values. The improved catalytic performance of the advanced VK58 catalyst will be further justified in molecular grounds in the light of the discussion of the Raman spectra in the next section. It appears, furthermore, that T_b is not affected by the water vapor content of the feed gas for VK38 and VK58, whereas it decreases by more than 35 °C in the case of VK-WSA. Finally it should be pointed out that as before [24], the data in Fig. 1 do not show the specific activity exactly and thus cannot be used to compare the maximum obtainable activities, because the availability of the active vanadium components is not fully determined by the amount of V_2O_5 present in the catalyst melt [5,23]. On the other hand,

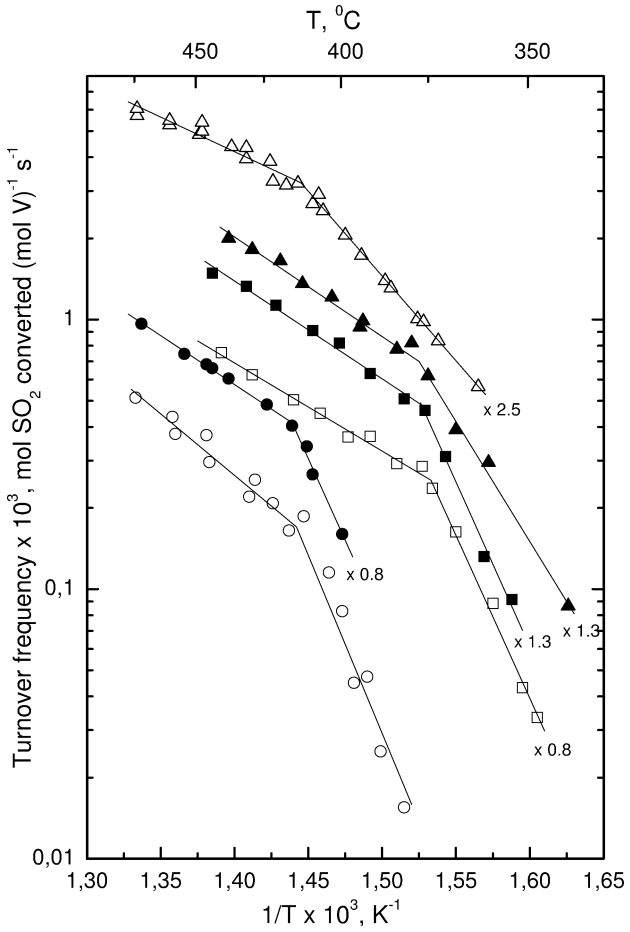

Fig. 1. Arrhenius plots for the mixed alkali-promoted industrial catalysts in dry feed gas (0.2% SO_2, 4.5% O_2, 15.1% CO_2, and 80.2% N_2), ○, VK38; □, VK58; △, VK-WSA, and wet feed gas (0.2% SO_2, 4% O_2, 7% H_2O, 14.1% CO_2, and 74.8% N_2) ●, VK38; ■, VK58; ▲, VK-WSA. For clarity, some of the plots are multiplied by the indicated factors.

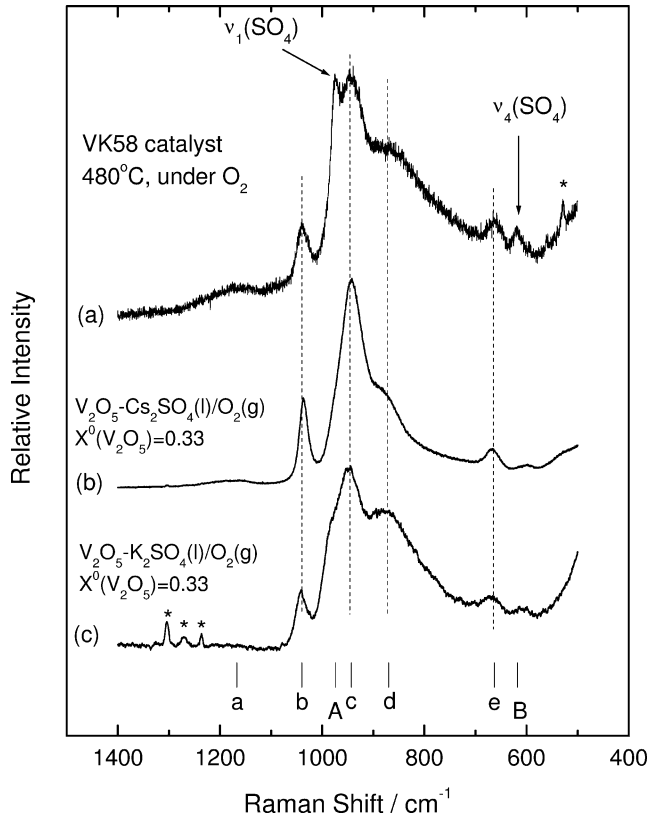

Fig. 2. (a) In situ Raman spectrum of VK58 (Na, K, Cs) catalyst at 480 °C under O_2. Laser wavelength, $\lambda_0 = 488.0$ nm; laser power, w = 25 mW; spectral slit width, ssw = 8 cm^{-1}; scan speed, ss = 0.15 $cm^{-1}\,s^{-1}$; time constant, $\tau = 2$ s. (b), (c) Raman spectra of V_2O_5–Cs_2SO_4 and V_2O_5–K_2SO_4 molten mixtures with $X^0_{V_2O_5} = 0.33$, obtained under O_2 at 490 °C. Asterisks (∗) mark laser plasma lines or grating ghosts.

the data can be used for the various catalysts and sets of conditions to compare the values of T_b at which the sharp drop of relative activity occurs and the molten salt catalyst undergoes phase transformation (precipitation).

3.2. In situ Raman spectra of oxidised catalysts after calcination

Following the synthesis procedure, the studied catalysts were calcined by the manufacturer (Haldor Topsøe A/S, Denmark). After calcination, the active components of the sulfuric acid catalysts are best represented by vanadium pentoxide and alkali sulfates [5]. Around 500 °C (i.e., below the calcination temperature), however, vanadium oxide reacts with alkali sulfates in the presence of oxygen and the reaction leads to a *molten salt* [19], which in the present case is expected to be dispersed and distributed at the surface of the inert catalyst carrier. It has been shown that a 2:1 M_2SO_4:V_2O_5 (M = K, Cs) mixture ($X^0_{V_2O_5} = 0.33$) melts below 450 °C and contains $VO_2(SO_4)_2^{3-}$ and VO_3^- units in chain-like and network-like configurations, whereas further addition of sulfate results in precipitation of crystalline M_2SO_4 [19]. It is worth noting the crucial role of the presence of oxygen, bearing in mind that as pointed out by Dearnaley and Kerridge [29], on the heating of such mixtures in the *absence* of oxygen a solid state reaction takes place, oxygen is released, and vanadium is partially reduced according to, e.g.,

$$K_2SO_4 + 6V_2O_5 \rightarrow 2KV_6O_{15} + \tfrac{1}{2}O_2 + SO_3. \quad (1)$$

In situ Raman spectra were recorded for the studied catalysts after 1 h of exposure to flowing O_2 at 480 °C and Fig. 2a shows the spectrum obtained for VK58 (spectra obtained for VK38 and VK-WSA were similar and are not shown, for brevity). The Raman spectra of *molten* V_2O_5–Cs_2SO_4 and V_2O_5–K_2SO_4 with $X^0_{V_2O_5} = 0.33$ obtained under O_2 at 490 °C are included for comparison (Figs. 2b and 2c) and are in agreement with the spectra reported previously [19]. A comparison of spectrum 2a with spectra 2b and 2c shows that the spectra of the VK58 catalyst (at 480 °C, under O_2) consist of superposition of bands due to V_2O_5–M_2SO_4 molten mixtures plus two bands at 974 and 618 cm^{-1}, which are due to the well-known [19] $\nu_1(SO_4^{2-})$ and $\nu_4(SO_4^{2-})$ modes of crystalline sulfate. It has previously been established that for $X^0_{V_2O_5} < 0.33$,

Table 2
Observed vibrational Raman wavenumbers (cm^{-1}) in in situ Raman spectra of VK58 catalyst and model molten salt mixtures[a]

Band notation (Fig. 2)	$V^{V}O_2(SO_4)_2^{3-}$ 490 °C Ref. [19] (K_2SO_4–V_2O_5)	VK58 catalyst (K/Cs/Na/V = 3/1/0.25/1) 480 °C, O_2	Assignments for catalyst (based on Ref. [19])	Band notation (Fig. 3)	$(V^{V}O)_2O(SO_4)_4^{4-}$ 450 °C Ref. [20] ($K_2S_2O_7$–V_2O_5)	VK58 catalyst (K/Cs/Na/V = 3/1/0.25/1) 380 °C, $SO_2 + O_2$	Assignments for catalyst (based on Refs. [18,20])
a	1168 w	1168 w, br	$V^{V}O_2(SO_4)_2^{3-}$,[b]	α	1180 m, br	1180 m, br	$(V^{V}O)_2O(SO_4)_4^{4-}$,[b]
				β	1050 s	1048 m	ν(V=O), $(V^{V}O)_2O(SO_4)_4^{4-}$
b	1042 s	1041 s	ν(V=O), $V^{V}O_2(SO_4)_2^{3-}$	b		1041 w	ν(V=O), $V^{V}O_2(SO_4)_2^{3-}$
				γ	1000 m	994 m	ν(S–O_t), $(V^{V}O)_2O(SO_4)_4^{4-}$
A		974 s, sharp	$\nu_1(SO_4^{2-})$, M_2SO_4 (cr)			965 w	$\nu(SO_4^{2-})$, $V^{IV}O(SO_4)_2^{2-}$
c	940 s	943 s	$\nu(SO_4^{2-})$, $V^{V}O_2(SO_4)_2^{3-}$	c		943 w	$\nu(SO_4^{2-})$, $V^{V}O_2(SO_4)_2^{3-}$
d	880 br	872 s, br	ν(S–O_b), $V^{V}O_2(SO_4)_2^{3-}$				
				δ	830 s, br	845 s, br	ν(S–O_b), $(V^{V}O)_2O(SO_4)_4^{4-}$
				ε	770 m	770 m, br	ν(V–O–V), $(V^{V}O)_2O(SO_4)_4^{4-}$
						700 w	
				ζ		686 m	$(V^{V}O)_2O(SO_4)_4^{4-}$,[c]
e	668 m	663 m	$V^{V}O_2(SO_4)_2^{3-}$,[c]		676 w	663 m	$(V^{V}O)_2O(SO_4)_4^{4-}$, $V^{V}O_2(SO_4)_2^{3-}$,[c]
B		618 m	$\nu_4(SO_4^{2-})$, M_2SO_4 (cr)		611 w	616 w	$(V^{V}O)_2O(SO_4)_4^{4-}$,[c]
	603 w			η	582 m	592 w	$(V^{V}O)_2O(SO_4)_4^{4-}$,[c]
	534 w				486 m		
	408 s				393		
	282 w				302 s		
	226 s				196		

[a] Abbreviations: s = strong; m = medium; w = weak; v = very; sh = shoulder; br = broad.
[b] Assigned to $\nu_3(SO_4)$ split components.
[c] Assigned either to $\nu_4(SO_4)$ split components or ν(V–O–).

crystalline M_2SO_4 (M = K, Cs) precipitates from V_2O_5–M_2SO_4/O_2 molten mixtures [19]. Therefore, alkali sulfate precipitation is indeed justified, since the active phase of the VK58, VK38, and VK-WSA catalysts contain 19, 20.8, and 20.8 mol% V_2O_5, respectively (see Table 1), i.e., much less than 33 mol%. The rest of the spectral features in Fig. 2a include bands at ∼ 1168 (weak, broad), 1041 (strong), 943 (strong), ∼ 872 (broad and strong), and 663 (medium) cm^{-1}. Significantly, bands at 1166–1168, 1036–1042, 940–941, ∼ 880, and 668 cm^{-1} are known to originate from the molten V^V complex $VO_2(SO_4)_2^{3-}$, which is a product of the reaction of V_2O_5 and M_2SO_4 (M = K, Cs) in the molten state [19], written as

$$V_2O_5 + 2SO_4^{2-} \rightarrow VO_2(SO_4)_2^{3-} + VO_3^{-}. \quad (2)$$

Naturally, since the state of the vanadium oxide present cannot be described accurately as V_2O_5, reaction (2) has to be considered only as a scheme accounting for the formation of molten $VO_2(SO_4)_2^{3-}$ at the catalyst surface. For the same reason it might be more appropriate to symbolize the second product of reaction (2) as VO_x. Table 2 (columns 1–4) lists the Raman band wavenumbers and their assignments for the in situ Raman spectrum of the calcined VK58 catalyst under O_2 at 480 °C and includes the Raman frequencies of the molten $VO_2(SO_4)_2^{3-}$ complex for comparison.

One should expect to observe the group vibrations of VO_2^{+} and SO_4^{2-} units of the $VO_2(SO_4)_2^{3-}$ V^V complex. The four sulfate fundamentals (ν_1–ν_4) for a tetrahedral T_d configuration span the representation

$$\Gamma_{vib} = A_1(\nu_1) + E(\nu_2) + 2F_2(\nu_3 + \nu_4)$$

and are well known from Raman work on aqueous solutions: $\nu_1(A_1) \approx 980$ cm^{-1}, $\nu_2(E) \approx 450$ cm^{-1}, $\nu_3(F_2) \approx 1100$ cm^{-1}, and $\nu_4(F_2) \approx 615$ cm^{-1} [30]. However, coordination of the sulfate ion and interactions with other ions are expected to shift the bands moderately, reduce the symmetry, and lift the degeneracies of the ν_2, ν_3, and ν_4 modes. This behavior has already been observed in the Raman spectra of molten M_2SO_4–V_2O_5, $M_2S_2O_7$–V_2O_5, and $M_2S_2O_7$–M_2SO_4–V_2O_5 (M = K or Cs) mixtures [18–20]. Vertical lines in Fig. 2 above the abscissa axis mark the most prominent bands due to the various species present as follows: uppercase A–B denote bands due to crystalline sulfate; lowercase a–e denote bands due to $VO_2(SO_4)_2^{3-}$ and this notation is maintained in Table 2. The band at 1041 cm^{-1} is due to the V^V=O terminal stretch of six-coordinated vanadium of $VO_2(SO_4)_2^{3-}$ and the shoulder band at 943 cm^{-1} is due to S–O terminal stretches of sulfate in $VO_2(SO_4)_2^{3-}$ [19]. The strong shoulder band at ∼ 872 cm^{-1} has previously [19] been assigned to S–O bridging modes along S–O–V chains of three-dimensional network-like $[VO_2(SO_4)_2]_n^{3n-}$ polymeric (or oligomeric) configurations formed in the molten salt mixtures [19].

3.3. In situ Raman spectra of catalysts in $SO_2/O_2/N_2$, SO_2/N_2, and $SO_2/H_2O/N_2$ atmospheres

3.3.1. Catalysts during reaction in $SO_2/O_2/N_2$ atmosphere

Figs. 3 and 4 show sequential in situ Raman spectra of the VK58 and VK38 catalysts, respectively, under $SO_2/O_2/N_2$ atmosphere obtained at different temperatures in the range 480–350 °C. The behavior of the VK-WSA was similar to VK38 and is not shown, for brevity.

Fig. 3 includes, for comparison, the in situ spectrum of the calcined VK58 catalyst under O_2 at 480 °C (spectrum 3a) and the Raman spectrum of the V_2O_5–$Cs_2S_2O_7$ molten salt mixture with $X^0_{V_2O_5} = 0.24$, obtained in O_2 atmosphere (spectrum 3f, reproduced from Ref. [18]). Spectrum 3b is obtained after exposure of VK58 to $SO_2/O_2/N_2$ at 480 °C for 1 h. The retention time of the gaseous reactants in the Raman furnace is sufficiently low to secure that SO_2 is converted to SO_3. Sulfur trioxide in turn reacts with crystalline alkali sulfate, which (as shown in the preceding section) is contained in the freshly calcined catalyst forming

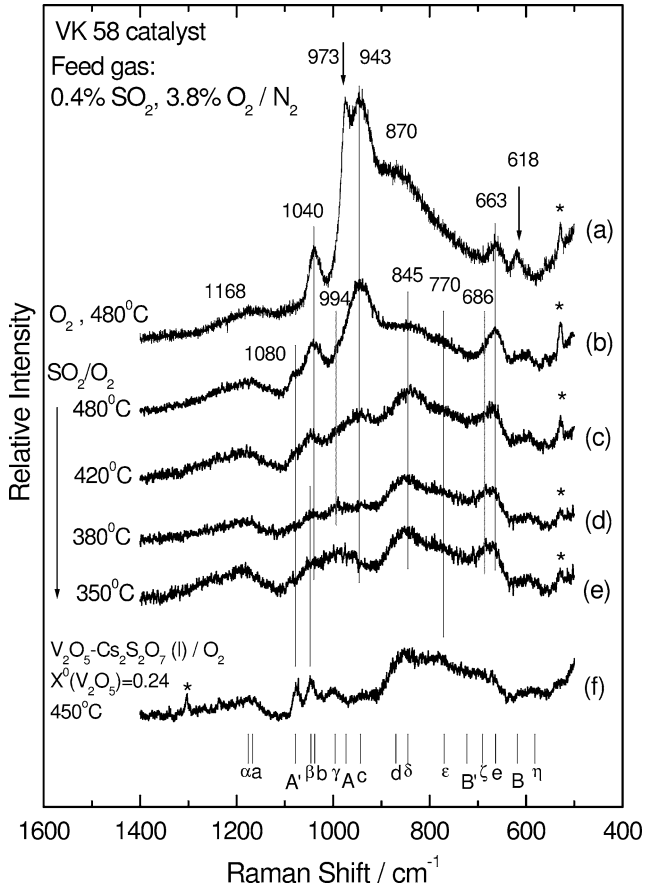

Fig. 3. (a)–(e) Sequential in situ Raman spectra of VK58 (Na, K, Cs) catalyst recorded at temperatures and gas atmospheres listed by each spectrum. $\lambda_0 = 488.0$ nm; w = 25 mW; ssw = 8 cm^{-1}; ss = 0.15 cm^{-1} s^{-1}; $\tau = 2$ s. (f) Raman spectrum of V_2O_5–$Cs_2S_2O_7$ molten mixture with $X^0_{V_2O_5} = 0.24$, obtained under O_2 at 450 °C (reproduced from Ref. [20]). Asterisks (∗) mark laser plasma lines or grating ghosts.

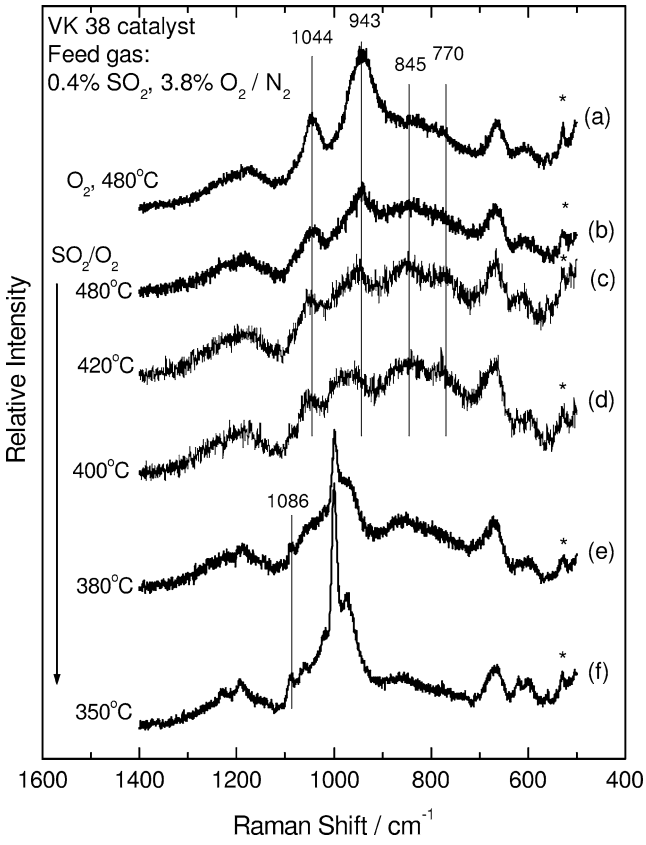

Fig. 4. (a)–(f) Sequential in situ Raman spectra of VK38 (Na, K) catalyst recorded at temperatures and gas atmospheres listed by each spectrum. $\lambda_0 = 488.0$ nm; w = 25 mW; ssw = 8 cm^{-1}; ss = 0.15 $cm^{-1}\,s^{-1}$; $\tau = 2$ s. Asterisks (∗) mark laser plasma lines.

molten pyrosulfate according to

$$SO_4^{2-} + SO_3 \rightarrow S_2O_7^{2-}. \quad (3)$$

Thus, as seen in Fig. 3b, bands A and B at 973 and 618 cm^{-1}, which were due to the ν_1 and ν_4 modes of crystalline sulfate, disappear. Moreover, SO_3 and $S_2O_7^{2-}$ react with the V^V oxosulfato complexes and/or the residual vanadium (V) oxides found at the catalyst surface according to [18,20]

$$V_2O_5 + 2S_2O_7^{2-} \rightarrow \left(V^VO\right)_2O(SO_4)_4^{4-}, \quad (4)$$

$$2V^VO_2(SO_4)_2^{3-} + 2SO_3 \rightarrow \left(V^VO\right)_2O(SO_4)_4^{4-} + S_2O_7^{2-}, \quad (5)$$

and indeed the characteristic 770/845 cm^{-1} strong and broad feature due to the molten dimeric $(V^VO)_2O(SO_4)_4^{4-}$ appears [18,20]. The 845 cm^{-1} band is due to bridging S–O along S–O–V and the 770 cm^{-1} band is due to V–O–V of the $(V^VO)_2O(SO_4)_4^{4-}$ molten complex [18,20], which is considered the active species in the catalytic cycle of SO_2 oxidation [6]. In order to facilitate the discussion, the spectrum of the V_2O_5–$Cs_2S_2O_7$ molten mixture with $X^0_{V_2O_5} = 0.24$ (i.e., merely a mixture of the $(V^VO)_2O(SO_4)_4^{4-}$ molten complex and $S_2O_7^{2-}$) at 450 °C is displayed in Fig. 3f. A weak band, seen at 1080 cm^{-1} in Fig. 3b, is due to $\nu_1(S_2O_7^{2-})$, which is the strongest band of the pyrosulfate ion [20], indicating the presence of small amounts of $S_2O_7^{2-}$ in solution.

Lowering of the temperature from 480 to 420, 380, and 350 °C under SO_2 and O_2 and recording of in situ Raman spectra after at least 1 h of exposure of the VK58 catalyst to the feed gas results in the following changes observed in the spectra shown in Figs. 3c, 3d, and 3e: (a) gradual blue shift of the 1041 cm^{-1} band (band b) due to the $V^V{=}O$ terminal stretch of $V^VO_2(SO_4)_2^{3-}$ to 1048 cm^{-1} (band β), where the $V^V{=}O$ terminal stretch of $(V^VO)_2O(SO_4)_4^{4-}$ is known to occur [18–20]; (b) weakening of the 943 cm^{-1} band (band c) of $V^VO_2(SO_4)_2^{3-}$, which vanishes around 380 °C; (c) strengthening of the 770/845 cm^{-1} broad feature (bands δ and ε); (d) appearance of bands at 994 and 686 (bands γ and ζ) due to terminal S–O stretch and $\nu_4(SO_4^{2-})$ split component of $(V^VO)_2O(SO_4)_4^{4-}$ [18,20]; and (e) appearance of a broad peak mass around 965 cm^{-1} at 350 °C (spectrum 3e), which has previously been assigned as due to the V^{IV} oxosulfato complex $V^{IV}O(SO_4)_2^{2-}$ [20]. Thus, it is evident that increasing amounts of the dimeric $(V^VO)_2O(SO_4)_4^{4-}$ are formed below 450 °C at the expense of the monomeric $V^VO_2(SO_4)_2^{3-}$, whereas below 380 °C the V^V complex undergoes partial reduction to V^{IV} according to [20,26,27]

$$\left(V^VO\right)_2O(SO_4)_4^{4-} + SO_2 \leftrightarrow 2V^{IV}O(SO_4)_2^{2-} + SO_3. \quad (6)$$

It appears, therefore, that even at temperatures below 380 °C a large amount of vanadium is stabilized in the +5 oxidation state and—significantly—in the form of the dimeric $(V^VO)_2O(SO_4)_4^{4-}$ complex, which has been identified as the catalytically active species during SO_2 oxidation [6]. Thus, the high catalytic activity and the improved low-temperature catalytic behavior (see Fig. 1) of VK58, which is an advanced catalyst promoted by a mixture of Na, K, and Cs, is fully justified in terms of high content of $(VO)_2O(SO_4)_4^{4-}$ and provides further evidence that $(VO)_2O(SO_4)_4^{4-}$ is the catalytically active species, as suggested earlier [6].

Increasing the temperature to 480 °C under SO_2 and O_2 restores the catalyst in its *activated* state, i.e., the one represented by the in situ Raman spectrum 3b. This is justified by the fact that at 480 °C reaction (3) is still shifted far to the right. Thus, cycling of the catalyst in the temperature range 480 → 350 → 480 °C leads to reproduction of spectra 3b–3e. The most prominent bands due to the various species present are listed in Table 2 (columns 5–8) together with their assignments and are marked by vertical lines in Fig. 3, where lowercase Greek letters α–η denote bands due to $(V^VO)_2O(SO_4)_4^{4-}$. A′ and B′ mark the positions of bands due to $S_2O_7^{2-}$ [20]. A, B, and a–e denote bands due to crystalline M_2SO_4 and molten $V^VO_2(SO_4)_2^{3-}$, as stated above.

Fig. 4 shows the evolution of the in situ Raman spectra obtained for the VK38 catalyst following sequential runs under $SO_2/O_2/N_2$ atmosphere at various temperatures in the range 480 → 350 °C. At each temperature, the catalyst

has been exposed to the feed gas for more than 1 h before the in situ Raman spectra are recorded. Spectrum 4a is obtained under pure flowing O_2 at 480 °C after the catalyst has been subjected to a full operation cycle consisting of stepwise lowering of the temperature in the range 480 → 350 °C and reheating to 480 °C. Thus, in the beginning of the cycle illustrated in Fig. 4, spectrum 4a consists of superposition of bands due to the monomeric $V^VO_2(SO_4)_2^{3-}$ (bands at 1179, 1044, 943, and 664 cm^{-1}) and due to the dimeric $(V^VO)_2O(SO_4)_4^{4-}$ (characteristic broad 845/770 cm^{-1} feature). Judged from the relative intensities of the bands it appears that at 480 °C under O_2 the $V^VO_2(SO_4)_2^{3-}$ is the predominant species in the molten salt mixture distributed at the surface of the VK38 catalyst. Exposure of the catalyst to the reacting $SO_2/O_2/N_2$ gas mixture at 480 °C (Fig. 4b) results in weakening of the 1044 and 943 cm^{-1} bands due to $V^VO_2(SO_4)_2^{3-}$ and appearance of the 1055 cm^{-1} band and strengthening of the 845/770 cm^{-1} feature due to $(V^VO)_2O(SO_4)_4^{4-}$. The observed changes are interpreted in terms of a shift of reaction (5) to the right. The assignment of the various bands has been presented in the previous sections and will not be discussed again. Small variations in the various wavenumbers are due to differences in the counter cations and has been observed also in Raman studies of the relevant unsupported molten salts [18–20].

The $(V^VO)_2O(SO_4)_4^{4-}$ complex becomes the dominant species when the temperature is lowered to 420 °C (Fig. 4c), as evidenced from the further strengthening of its spectral features relative to the 943 cm^{-1} $V^VO_2(SO_4)_2^{3-}$ band. However, further lowering of the temperature to 400 °C (Fig. 4d) gives rise to a peak mass centered at ∼ 965 cm^{-1}, which is characteristic of the V^{IV} complex $V^{IV}O(SO_4)_2^{2-}$ [20] formed according to reaction (6). It is evident that already at 400 °C a portion of vanadium occurs in the +4 oxidation state, a fact that explains why the precipitation of V^{IV} crystalline compounds occurs at higher temperature for the VK38 compared to VK58 (Fig. 1, Table 1). It is well established that below a certain temperature, when V^{IV} concentration exceeds its solubility limit, precipitation of V^{IV} crystalline compounds leads to catalyst deactivation by depleting the active molten phase in terms of vanadium [6,25]. Indeed, further lowering of the temperature to 380 and 350 °C (Figs. 4e and 4f) results in weakening of the bands due to the V^V species $(V^VO)_2O(SO_4)_4^{4-}$ and to the appearance of the very characteristic sharp bands at 999 and 973 cm^{-1} which are due to the V^{IV} crystalline compound $K_4(VO)_3(SO_4)_5$ [31], which precipitates and has been identified as the most common deactivation product of sulfuric acid catalysts [6,24,25,32]. Further evidence and discussion on the route leading to precipitation of $K_4(VO)_3(SO_4)_5$ will be given in the next section dealing with in situ Raman spectra in reducing conditions, i.e., in SO_2/N_2 atmosphere.

3.3.2. Raman spectra in reducing conditions (SO_2/N_2 atmosphere)

Figs. 5 and 6 show sequential in situ Raman spectra of the VK58 and VK38 catalysts, respectively, in reducing conditions, i.e., at SO_2/N_2 atmosphere obtained at different temperatures in the range 480–350 °C. The behavior of the VK-WSA was similar to that of VK38 and is not shown, for brevity.

Spectrum 5a is obtained for the VK58 catalyst after it has been subjected to a full operation cycle at $SO_2/O_2/N_2$ atmosphere consisting of stepwise lowering of the temperature in the range 480 → 350 °C and reheating at 480 °C. As before (see Fig. 3b and relevant discussion in preceding section) the active liquid phase of the catalyst is a molten salt mixture consisting of the V^V complexes $VO_2(SO_4)_2^{3-}$ and $(VO)_2O(SO_4)_4^{4-}$ and a small amount of $S_2O_7^{2-}$. After the flow of oxygen is switched off and the VK58 catalyst is exposed to an SO_2/N_2 atmosphere at 480 °C for 1 h the obtained Raman spectrum (Fig. 5b) does not show appreciable differences when compared to spectrum 5a, indicating (as expected) that at 480 °C under an SO_2 atmosphere vanadium is still stable in its +5 oxidation state. Likewise, no changes occurred till the temperature was lowered to 420 °C,

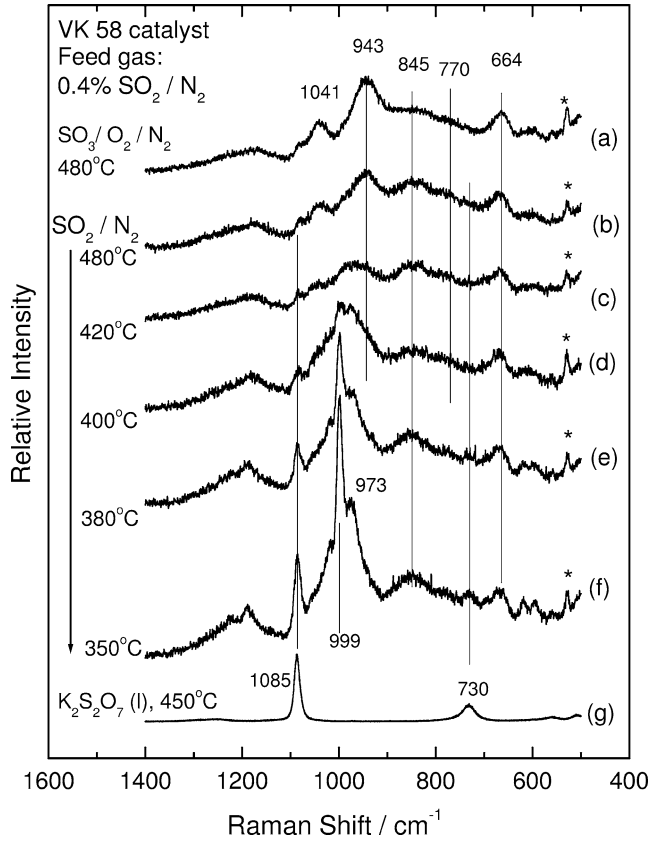

Fig. 5. (a)–(f) Sequential in situ Raman spectra of VK58 (Na, K, Cs) catalyst recorded at temperatures and gas atmospheres listed by each spectrum. $\lambda_0 = 488.0$ nm; w = 25 mW; ssw = 8 cm^{-1}; ss = 0.15 cm^{-1} s^{-1}; $\tau = 2$ s. (g) Raman spectrum of molten $K_2S_2O_7$, obtained under O_2 at 450 °C (reproduced from Ref. [20]). Asterisks (∗) mark laser plasma lines.

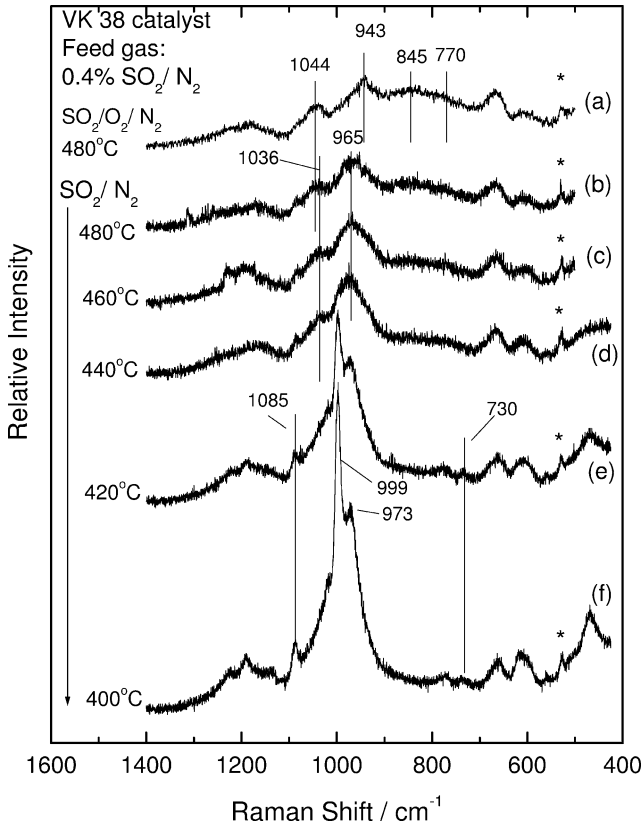

Fig. 6. (a)–(f) Sequential in situ Raman spectra of VK38 (Na, K) catalyst recorded at temperatures and gas atmospheres listed by each spectrum. $\lambda_0 = 488.0$ nm; w = 25 mW; ssw = 8 cm^{-1}; ss = 0.15 $cm^{-1}\,s^{-1}$; $\tau = 2$ s. Asterisks (∗) mark laser plasma lines.

where the first characteristic indications of $V^V \rightarrow V^{IV}$ reduction can be recognized in spectrum 5c. Indeed, the characteristic features of the V^{IV} complex $V^{IV}O(SO_4)_2^{2-}$ [20] at ∼ 965 cm^{-1} (sulfate mode) and 1038 (V^{IV}=O mode) cm^{-1} are seen. Now, the assignment of the band in the vicinity of 1038 cm^{-1} needs to be careful, since at 1041 cm^{-1} the V^V=O of the $V^VO_2(SO_4)_2^{3-}$ occurs as well. However, judged from the vanishing of the 943 cm^{-1} $V^VO_2(SO_4)_2^{3-}$ band and the red shift of the 1041 cm^{-1} V^V=O band (spectrum 5b) to 1038 cm^{-1} (spectrum 5c) it can be concluded that the 1038 cm^{-1} band belongs to the V^{IV} complex, formed, e.g., according to reaction (6). It is noteworthy that in spectrum 5c, obtained at 420 °C under an SO_2/N_2 atmosphere, the 965 cm^{-1} $V^{IV}O(SO_4)_2^{2-}$ band [20] has emerged, whereas the 943 cm^{-1} $V^VO_2(SO_4)_2^{3-}$ band has disappeared, indicating a significant extent of $V^V \rightarrow V^{IV}$ reduction. In fact, when oxygen was present as well (i.e., in an $SO_2/O_2/N_2$ atmosphere) a similar extent of reduction was observed at least 70 °C lower, at 350 °C. This is judged, based on the similarities of spectrum 5c with spectrum 3e obtained at 350 °C under $SO_2/O_2/N_2$ atmosphere. This is not surprising in view of the fact that the absence of oxygen, which would convert SO_2 to SO_3, results in a higher partial pressure of SO_2, thereby shifting the $V^V \rightarrow V^{IV}$ reduction [e.g., reaction (6)] to the right.

Further lowering of the temperature to 400 °C (spectrum 5d) results in changes that are interpreted to indicate that precipitation of V^{IV} has already commenced. The observed changes include: (a) appearance of the 999 cm^{-1} characteristic band of crystalline $K_4(VO)_3(SO_4)_5$ emerging from the broad peak mass centered around 980 cm^{-1}; and (b) strengthening of the 1085 cm^{-1} $\nu_1(S_2O_7^{2-})$ band. Further lowering of the temperature, to 380 °C (spectrum 5e) and 350 °C (spectrum 5f), results in formation of larger amounts of crystalline $K_4(VO)_3(SO_4)_5$, whereas the simultaneous increase of the 1085 cm^{-1} $\nu_1(S_2O_7^{2-})$ band together with the appearance of a band at 730 cm^{-1}, where the second strongest $S_2O_7^{2-}$ band occurs in the studied wavenumber region, points to formation of increased amounts of pyrosulfate. The Raman spectrum of molten potassium pyrosulfate [20] is reproduced in Fig. 5g for comparison.

The above observations can be interpreted in terms of the following reactions, which summarize the mechanism of deactivation of the supported molten salt catalysts for SO_2 oxidation:

$$3\left(V^VO\right)_2O(SO_4)_4^{4-} + 3SO_2 + 8K^+ \rightarrow 2K_4\left(V^{IV}O\right)_3(SO_4)_5(s) + 2S_2O_7^{2-} + SO_3, \quad (7)$$

$$3V^{IV}O(SO_4)_2^{2-} + SO_3 + 4K^+ \rightarrow K_4\left(V^{IV}O\right)_3(SO_4)_5(s) + S_2O_7^{2-}. \quad (8)$$

Reactions (7) and (8) include a $V^V \rightarrow V^{IV}$ reduction step, a combination of ligands resulting to precipitation of the blue V^{IV} compound $K_4(VO)_3(SO_4)_5$, and liberation of pyrosulfate solvent. This scheme describes exactly the deactivation route of the sulfuric acid catalysts, resulting in depletion of the catalyst melts from their active component, during which vanadium comes out of the molten phase in a nonactive tetravalent state and the remaining liquid contains larger amounts of inactive components (i.e., pyrosulfate).

Fig. 6 shows the evolution of the in situ Raman spectra of the VK38 catalyst in an SO_2/N_2 atmosphere at various temperatures in the range 480 → 400 °C, following exposure of the catalyst in temperature and gas feed conditions shown next to each spectrum for more than 1 h. In the beginning of the sequence illustrated in Fig. 6 (spectrum 6a) the catalyst is in *activated* form; i.e., it has been subjected to an $SO_2/O_2/N_2$ atmosphere at 480 °C after a full operation cycle in an $SO_2/O_2/N_2$ atmosphere (consisting of stepwise lowering of the temperature in the range 480 → 350 °C—as shown in Fig. 4—and reheating at 480 °C). Thus, as stated above, the liquid phase of the catalyst is a mixture of the mononuclear $V^VO_2(SO_4)_2^{3-}$ and the dinuclear $(V^VO)_2O(SO_4)_4^{4-}$ complexes. After the flow of O_2 is switched off and the VK38 catalyst is exposed to SO_2/N_2 flowing gas at 480 °C, the Raman spectrum (Fig. 6b) shows that extensive $V^V \rightarrow V^{IV}$ reduction has occurred, as indicated by: (a) vanishing of the 943 cm^{-1} $V^VO_2(SO_4)_2^{3-}$ band; (b) lowering of the 845/770 cm^{-1}

broad $(V^{V}O)_2O(SO_4)_4^{4-}$ band; (c) appearance of a peak mass centered at 965 cm^{-1} due to V^{IV} species (e.g., $V^{IV}O(SO_4)_2^{2-}$ [20]); and (d) shift of the 1055/1044 cm^{-1} V^{V}=O feature of $(V^{V}O)_2O(SO_4)_4^{4-}$ and $V^{V}O_2(SO_4)_2^{3-}$ to 1036 cm^{-1}, where the V^{IV}=O band of the V^{IV} species occurs [20]. Reaction schemes accounting for the above observations include Eq. (6) and

$$2V^{V}O_2(SO_4)_2^{3-} + SO_2 \leftrightarrow V^{IV}O(SO_4)_2^{2-} + V^{IV}O(SO_4)_3^{4-}. \quad (9)$$

Spectra obtained after further lowering of the temperature to 460 and 440 °C (Figs. 6c and 6d) show that the V^{IV} species dominate completely. Thus, contrary to the case of VK58 catalyst (Fig. 5), where at 480 and even at 420 °C vanadium persists (at least to a significant extent) in the +5 state, VK38 undergoes an easy reduction. Therefore, it appears once again that mixing of alkali promoters in VK58 by inclusion of Cs [24,25] is very beneficial for the stability of V^{V} complexes, which are the catalytically active species during SO_2 oxidation [6,21]. The stability of V^{V} in Cs-promoted melts offers an improved low-temperature (e.g., below 420 °C) activity for the VK58 catalyst compared to VK38 (which is promoted by K, Na). This is in agreement with the relative positions of the break points in the Arrhenius plots of the apparent reaction rates obtained in the present work (Fig. 1 and Table 1).

Below 420 °C, large amounts of the crystalline V^{IV} compound $K_4(VO)_3(SO_4)_5$ precipitate in the liquid catalyst phase, as indicated by the presence of the characteristic 999/973 cm^{-1} sharp bands in Figs. 6e and 6f and by the emergence of the 1085 and 730 cm^{-1} pyrosulfate bands.

The observed differences in the relative intensities of the bands due to $S_2O_7^{2-}$ in spectra 5f and 6f can be due to the difference in the initial amounts of alkali sulfates between VK58 and VK38. VK58 contains around 12 mol% more alkali promoters than VK38 ($M/V = 4.25$ compared to $M/V = 3.8$ for VK38), which results in a higher content of pyrosulfate solvent after SO_3 uptake.

3.3.3. In situ Raman spectra in the presence of water vapors

Industrial experience with the Haldor Topsøe VK catalysts has revealed that the presence of water vapor in sulfuric acid synthesis gas has a well-pronounced beneficial effect in low-temperature catalytic activity [1]. The observed effect was so significant that it allowed the reactors to operate at temperatures 20–30 °C lower when compared to the conventional process, i.e., when water vapors are not present, and thus catalysts could operate without undergoing depletion of their active components, which would otherwise be caused by precipitation of V^{IV} and V^{III} compounds. The achievement of lower operation temperatures, in turn, shifted equilibrium for the exothermic reaction $SO_2 + \frac{1}{2}O_2 \rightarrow SO_3$ further to the right and allowed attainment of much lower SO_2 content in the stack gas. The so-called WSA (wet sulfuric acid) process was then proposed and launched to help the single-absorption sulfuric acid plants to comply with environmental legislation.

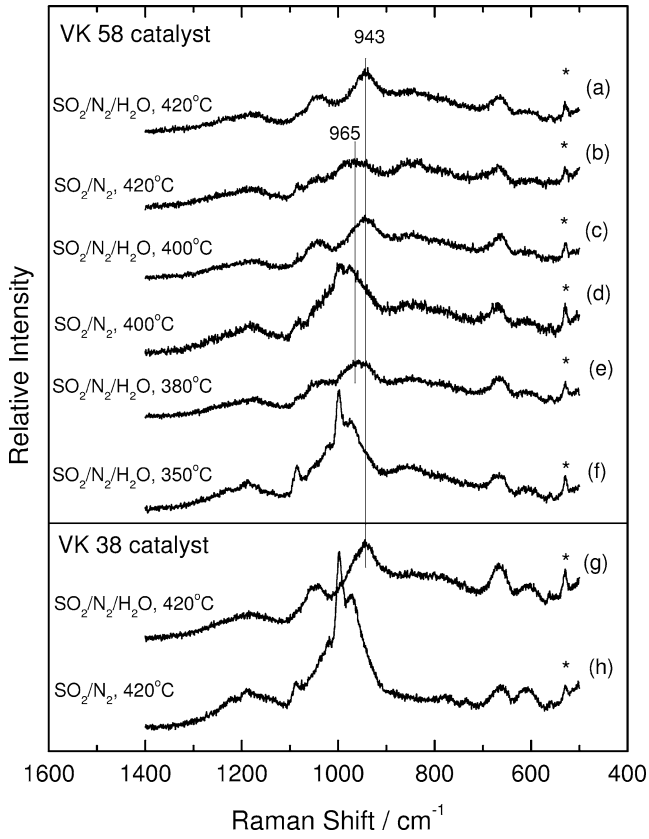

Fig. 7. In situ Raman spectra of VK58 (Na, K, Cs) catalyst (spectra a–f) and VK38 (Na, K) catalyst (spectra g, h) recorded at temperatures and gas atmospheres listed by each spectrum. $\lambda_0 = 488.0$ nm; w = 25 mW; ssw = 8 cm^{-1}; ss = 0.15 $cm^{-1}s^{-1}$; $\tau = 2$ s. Asterisks (∗) mark laser plasma lines.

The presence of water vapor is expected to modify the identity of the ligands present in the molten salt solution that constitutes the active phase of the SO_2 oxidation catalyst, since water vapors are taken up, e.g., according to $S_2O_7^{2-} + H_2O \rightarrow 2HSO_4^{-}$ [33].

In order to examine the effect of water vapors on the catalyst behavior, in situ Raman spectra were obtained for the studied catalysts under an $SO_2/H_2O/N_2$ gas atmosphere. A portion of the carrier gas (N_2) was passed through water contained in two bottles connected in series and immersed in a 51 °C-controlled thermostat. In this way, after the dry SO_2/N_2 stream was mixed with the wetted N_2 stream the resulting feed gas contained 8% water vapors. Fig. 7 shows representative in situ Raman spectra obtained for VK58 and VK38 in selected temperatures under an $SO_2/H_2O/N_2$ atmosphere. Selected spectra obtained in dry conditions are included for comparison. Before the spectra were obtained in wet conditions, the catalysts were subjected to a few full operation cycles under $SO_2/O_2/N_2$ and SO_2/N_2 atmospheres, consisting of stepwise lowering of the temperature in the range 480–350 °C, reheating under O_2 at 480 °C, and reac-

tivation under $SO_2/O_2/N_2$ at 480 °C. In situ Raman spectra of the reactivated catalysts were then recorded at 480 °C and were found to be identical to spectra 5a and 6a for VK58 and VK38, respectively. The flow of oxygen was then switched off and the SO_2/N_2 stream was wetted as described above. The in situ Raman spectra obtained after the catalysts were exposed to an $SO_2/H_2O/N_2$ atmosphere at various temperatures in the range 480–440 °C did not show appreciable differences when compared to the corresponding spectra obtained in the absence of water vapor. However, the situation changes dramatically at and below 420 °C. Spectrum 7a is obtained at 420 °C for the VK58 catalyst after 1 h of exposure to $SO_2/H_2O/N_2$ and is compared to spectrum 7b (reproduced from Fig. 5c) obtained in the absence of H_2O(g). It is evident that, whereas in the absence of H_2O(g) the spectra are indicative of $V^V \rightarrow V^{IV}$ reduction (as described in the relevant section above), in the presence of H_2O(g) the catalyst remains stable, with vanadium in the +5 state, judged from the presence of bands which are due either to $V^VO_2(SO_4)_2{}^{3-}$ (943, 1041 cm^{-1}) or to $(V^VO)_2O(SO_4)_4{}^{4-}$ (845/770 cm^{-1}). At 400 °C the comparison is even clearer. Spectrum 7c (obtained at 400 °C for the VK58 catalyst under $SO_2/H_2O/N_2$) reveals that the V^V complexes are still stable (as there are no differences when compared to spectrum 7a). In the absence of H_2O(g) (spectrum 7d, reproduced from Fig. 5d) most of the vanadium is in the +4 state, as discussed above in the relevant section. Finally, at 380 °C under $SO_2/H_2O/N_2$ the indications that $V^V \rightarrow V^{IV}$ reduction is initiated can be recognized in spectrum 7e, i.e., shift of the peak mass from 943 to 965 cm^{-1} (sulfate mode of $V^{IV}O(SO_4)_2{}^{2-}$) and appearance of 1038 cm^{-1} V^{IV}=O mode. However, at the same temperature in the absence of water vapor extensive V^{IV} precipitation mainly in the form of $K_4(VO)_3(SO_4)_5$ was observed for VK58 (spectrum 5e), which is seen at 350 °C (i.e., 30 °C lower) in the presence of water vapor (spectrum 7f) as recognized from the characteristic 999/983 cm^{-1} sharp doublet. The identity of the precipitating compound was checked also by ESR. The ESR spectrum of the VK58 catalyst, after being subjected to $SO_2/H_2O/N_2$ and cooled at room temperature, possessed a sharp narrow line characteristic of $K_4(VO)_3(SO_4)_5$ with isotropic *g*-value 1.965 and linewidth 119.2 G, very close to what has been found for $K_4(VO)_3(SO_4)_5$ [25,32]. A similar situation is experienced also with VK38 and VK-WSA, e.g., as shown in Figs. 7g and 7h. Thus while, in the presence of H_2O(g) at 420 °C, VK38 exhibits excellent stability of the V^V complexes (spectrum 7g), extensive V^{IV} precipitation is experienced in the absence of water vapor (spectrum 7h, reproduced from Fig. 6e).

Thus, the presence of water vapor enhances the stability of V^V complexes and the industrially experienced improved low temperature catalyst activity can be explained in terms of higher contents of catalytically active V^V molten complexes as seen in the Raman spectra. Unfortunately, it was not possible to obtain in situ Raman spectra in $SO_2/O_2/H_2O/N_2$ atmosphere because of formation of sulphuric acid mist, the formation and condensation of which did not allow the operation of the in situ Raman cell. Therefore the spectra shown in Fig. 7, obtained in $SO_2/H_2O/N_2$ atmosphere, cannot be directly related with the part of the data of Fig. 1 obtained using the wet feed gas.

3.4. Molecular structure of sulphuric acid catalysts and relation to catalysis

The Raman spectra presented and discussed above show that: (i) in freshly calcined catalysts under O_2 the mononuclear $V^VO_2(SO_4)_2{}^{3-}$ species (in monomeric or oligomeric form) is predominant; (ii) after *activation* (treatment with $SO_2/O_2/N_2$) the binuclear $(V^VO)_2O(SO_4)_4{}^{4-}$ complex is formed; (iii) with decreasing temperature and/or increased SO_2 presence in the gas phase, $V^V \rightarrow V^{IV}$ reduction occurs, leading to formation of the $V^{IV}O(SO_4)_2{}^{2-}$ complex.

Fig. 8 shows the proposed structural models for the various V^V and V^{IV} species identified in the molten active phase of the industrial SO_2 oxidation catalysts studied. The configurations depicted in Fig. 8 have been proposed earlier, based on high-temperature Raman studies of the V_2O_5–$M_2S_2O_7$–M_2SO_4/O_2–SO_2 unsupported molten salt/gas "model" systems [18–20].

The most striking result is the predominance of the binuclear $(V^VO)_2O(SO_4)_4{}^{4-}$ complex in the liquid phase of the *activated* catalysts (i.e., after treatment with an SO_2/O_2 mixture). This result provides further evidence to support a recently proposed mechanism, which involves the $(V^VO)_2O(SO_4)_4{}^{4-}$ complex as the active species dur-

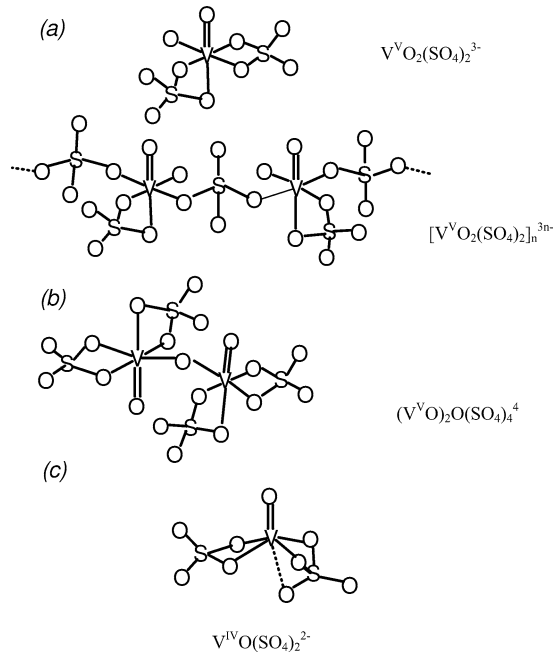

Fig. 8. Possible molecular structural models for the V complexes present in industrial SO_2 oxidation molten salt catalysts: (a) $V^VO_2(SO_4)_2{}^{3-}$ in monomeric and oligomeric form; (b) $(V^VO)_2O(SO_4)_4{}^{4-}$; and (c) $V^{IV}O(SO_4)_2{}^{2-}$.

ing SO_2 oxidation [6]. The bidentate sulfate ligands found within $(V^VO)_2O(SO_4)_4{}^{4-}$, Fig. 8b, are strained due to their unusual distortion and may open up, making the complex coordinatively unsaturated in the horizontal positions and leading to the suggested coordination of O_2 as the first step of the catalytic cycle: $(V^VO)_2O(SO_4)_4{}^{4-} + O_2 \leftrightarrow (V^VO)_2O(SO_4)_4O_2{}^{4-}$ [6]. Previously [20] it has been demonstrated that SO_2 does not coordinate with the V^V complex. Reduction of V^V by SO_2 is favored below a certain temperature and results in formation and accumulation of catalytically inactive V^{IV} complexes $V^{IV}O(SO_4)_2{}^{2-}$, Fig. 8c, leading to precipitation of V^{IV} crystalline compounds (mainly $K_4(VO)_3(SO_4)_5$) and deactivation of the catalysts [6,24,25].

4. Conclusions

Industrial SO_2 oxidation catalysts have been investigated by combined in situ Raman spectroscopy and catalytic activity measurements. The species present in the active liquid catalyst phase are identified from the Raman spectra. The molten phase of the freshly calcined catalysts contains predominantly the mononuclear $V^VO_2(SO_4)_2{}^{3-}$ complex (in monomeric or oligomeric form). During catalyst activation a pyrosulfate-containing molten salt is formed, leading to formation of the binuclear (dimeric) $(V^VO)_2O(SO_4)_4{}^{4-}$ complex, which has previously been proposed as the catalytically active species during SO_2 oxidation [6]. Below a certain temperature (which depends on gas conditions and catalyst composition) V^V is reduced to V^{IV}, the catalytic activity decreases, and V^{IV} compounds, mainly $K_4(VO)_3(SO_4)_5$, precipitate. Maintaining vanadium in the $+5$ state is the key to high catalytic activity since the catalytic cycle involves only V^V [6,21], whereas V^{IV} is involved in the deactivation route. High stability of V^V is achieved by: (a) mixing of alkali promoters; (b) inclusion of Cs as a promoter; and (c) the presence of water vapors in the feed gas. This investigation demonstrates the feasibility of studying supported molten salt catalysts for SO_2 oxidation by in situ Raman spectroscopy. The spectra obtained are used in conjunction with high-temperature spectra of model systems [18–20] to study the molecular structure of the catalysts.

Acknowledgments

NATO's Scientific Affairs Division in the framework of the Science for Peace Programme (SfP 971984) sponsored this research. Support from the General Secretariat of Research and Technology of the Greek Ministry of Development is gratefully acknowledged. Søren B. Rasmussen is thanked for recording the ESR spectrum. Many thanks to Haldor Topsøe A/S, Denmark (www.topsoe.dk), for providing the catalyst samples.

References

[1] D.J. Smith, Power Eng. Int. (April 21, 1994);
H. Jensen-Holm, O. Rud-Bendixen, Industrial Experience with the Topsoe VK 48 Sulfuric Acid Catalyst and the WSA-2 Process, presented at Sulfur, 1990, Cancun, Mexico.
[2] J.H. Frazer, W.J. Kirkpatrick, J. Am. Chem. Soc. 62 (1940) 1659.
[3] H.F.A. Topsoe, A. Nielsen, Trans. Dan. Acad. Tech. Sci. 1 (1947) 18.
[4] P. Mars, J.G.H. Maessen, J. Catal. 10 (1968) 1.
[5] H. Livbjerg, J. Villadsen, Catal. Rev. Sci. Eng. 17 (1978) 203.
[6] O.B. Lapina, B.S. Bal'zhinimaev, S. Boghosian, K.M. Eriksen, R. Fehrmann, Catal. Today 51 (1999) 469.
[7] O.B. Lapina, V.M. Mastikhin, A.A. Shubin, V.N. Krasilnikov, K.I. Zamaraev, Prog. NMR Spectrosc. 24 (1992) 457.
[8] V.M. Mastikhin, O.B. Lapina, in: Encyclopedia of Nuclear Magnetic Resonance, Vol. 8, Wiley, New York, 1996, p. 4892.
[9] V.M. Mastikhin, G.N. Polyakova, J. Ziolkowsky, G.K. Boreskov, Kinet. Katal. 1 (1970) 1463.
[10] S.V. Kozyrev, B. Bal'zhinimaev, G.K. Boreskov, A.A. Ivanov, V.M. Mastikhin, React. Kinet. Catal. Lett. 20 (1982) 53.
[11] G.K. Boreskov, Davydova, V.M. Mastikhin, G.N. Polyakova, Dokl. Akad. Nauk. SSSR Ser. Khim. 171 (1966) 648.
[12] N.H. Hansen, R. Fehrmann, N.J. Bjerrum, Inorg. Chem. 21 (1982) 744.
[13] R. Fehrmann, M. Gaune-Escard, N.J. Bjerrum, Inorg. Chem. 25 (1986) 1132.
[14] G. Hatem, R. Fehrmann, M. Gaune-Escard, N.J. Bjerrum, J. Phys. Chem. 91 (1987) 195.
[15] G. Folkmann, G. Hatem, R. Fehrmann, M. Gaune-Escard, N.J. Bjerrum, Inorg. Chem. 32 (1993) 1559.
[16] O.B. Lapina, V.M. Mastikhin, A.A. Shubin, K.M. Eriksen, R. Fehrmann, J. Mol. Catal. A Chem. 99 (1995) 123.
[17] I. Petrushina, N.J. Bjerrum, F. Cappeln, J. Electrochem. Soc. 145 (1998) 3721.
[18] S. Boghosian, F. Borup, A. Chrissanthopoulos, Catal. Lett. 48 (1997) 145.
[19] S. Boghosian, J. Chem. Soc. Faraday Trans. 94 (1998) 3463.
[20] S. Boghosian, A. Chrissanthopoulos, R. Fehrmann, J. Phys. Chem. B 106 (2002) 49.
[21] B. Bal'zhinimaev, A.A. Ivanov, O.B. Lapina, V.M. Mastikhin, K.I. Zamaraev, Faraday Discuss. Chem. Soc. 87 (1989) 133.
[22] G.K. Boreskov, L.P. Polyakova, A.A. Ivanov, V.M. Mastikhin, Dokl. Akad. Nauk. SSSR 210 (1973) 626.
[23] P. Grydgaard, H. Jensen-Holm, H. Livbjerg, J. Villadsen, ACS Sympos. Ser. 65 (1978) 582.
[24] S. Boghosian, R. Fehrmann, N.J. Bjerrum, G.N. Papatheodorou, J. Catal. 119 (1989) 121.
[25] K.M. Eriksen, D.A. Karydis, S. Boghosian, R. Fehrmann, J. Catal. 155 (1995) 32.
[26] D.A. Karydis, K.M. Eriksen, R. Fehrmann, S. Boghosian, J. Chem. Soc. Dalton Trans. (1994) 2151.
[27] S.B. Rasmussen, K.M. Eriksen, R. Fehrmann, J. Phys. Chem. B 103 (1999) 11282.
[28] S.G. Masters, A. Chrissanthopoulos, K.M. Eriksen, S. Boghosian, R. Fehrmann, J. Catal. 166 (1997) 16.
[29] R.I. Dearnaley, D.H. Kerridge, Thermochim. Acta 63 (1983) 219.
[30] K. Nakamoto, Infrared and Raman Spectra of Inorganic and Coordination Compounds, Wiley, New York, 1986.
[31] R. Fehrmann, S. Boghosian, G.N. Papatheodorou, K. Nielsen, R.W. Berg, N.J. Bjerrum, Inorg. Chem. 28 (1989) 1847.
[32] K.M. Eriksen, R. Fehrmann, N.J. Bjerrum, J. Catal. 132 (1991) 263.
[33] R. Fehrmann, N.H. Hansen, N.J. Bjerrum, Inorg. Chem. 22 (1983) 4009.